THE ASTROPHYSICAL JOURNAL, 562:593–604, 2001 December 1

DIRECT DETECTION OF WARM DARK MATTER IN THE X-RAY

KEVORK ABAZAJIAN,[1] GEORGE M. FULLER,[1] AND WALLACE H. TUCKER[1,2]

Received 2001 May 31; accepted 2001 July 31

ABSTRACT

We point out a serendipitous link between warm dark matter (WDM) models for structure formation on the one hand and the high-sensitivity energy range (1–10 keV) for X-ray photon detection on the *Chandra* and *XMM-Newton* observatories on the other. This fortuitous match may provide either a direct detection of the dark matter or the exclusion of many candidates. We estimate expected X-ray fluxes from field galaxies and clusters of galaxies if the dark matter halos of these objects are composed of WDM candidate particles with rest masses in the structure formation–preferred range (~ 1 to ~ 20 keV) and with small radiative decay branches. Existing observations lead us to conclude that for singlet neutrinos (possessing a very small mixing with active neutrinos) to be a viable WDM candidate they must have rest masses $\lesssim 5$ keV in the zero lepton number production mode. Future deeper observations may detect or exclude the entire parameter range for the zero lepton number case, perhaps restricting the viability of singlet neutrino WDM models to those where singlet production is driven by a significant lepton number. The Constellation X project has the capability to detect/exclude singlet neutrino WDM for lepton number values up to 10% of the photon number. We also consider diffuse X-ray background constraints on these scenarios. These same X-ray observations additionally may constrain parameters of active neutrino and gravitino WDM candidates.

Subject headings: dark matter — elementary particles — neutrinos — X-rays: diffuse background — X-rays: galaxies — X-rays: galaxies: clusters

1. INTRODUCTION

In this paper we show how the *Chandra*, *XMM-Newton*, and future Constellation X observatories can detect or exclude several warm dark matter (WDM) candidates, including singlet ("sterile") neutrinos, heavy active neutrinos, and gravitinos in some models. In essence, we show here how the technology of modern X-ray astronomy allows the exploration of a new sector of particle physics, one where interaction strengths could be characteristically some 10 orders of magnitude weaker than the weak interaction. Processes with these interaction strengths likely never could be probed directly in a laboratory.

The X-ray observatories, however, possess several advantages when it comes to probing WDM candidate particles. First, the sensitive energy range for X-ray photon detection on these instruments is ~ 1 to ~ 10 keV. Serendipitously, this is more or less coincident with the WDM candidate particle rest mass range that is preferred in studies of structure formation (Bode, Ostriker, & Turok 2001). Some models posit the production of WDM particles through their tiny interactions with ordinary matter. In several cases these very weak interactions lead to small radiative decay branches, producing photons with energies of order the WDM particle rest mass.

This is where the second advantage of X-ray astronomy comes in. Even though the WDM particle decay rate into photons can be very small (lifetimes against radiative decay are typically $\sim 10^{16} \times$ Hubble time), the dark matter halos of galaxies and galaxy clusters can contain huge numbers of particles, e.g., in the latter class of objects, some 10^{79} particles of rest mass ~ 1 keV. In effect, dark matter halos can serve as laboratories of enormous "fiducial volumes" of dark matter particles.

The first evidence for dark matter was the velocity dispersion of galaxies in the Coma Cluster, which required mass-to-light ratios in the cluster to exceed those inferred for our Galaxy by many times (Zwicky 1933). Later, observations of giant spiral galaxies implied that their disks are imbedded in larger halos of dark matter (Ostriker, Peebles, & Yahil 1974; Einasto, Kaasik, & Saar 1974). Recently, problems in cosmological structure formation models have led to interest in alternatives to the standard cold dark matter (CDM) model for structure formation.

The primary problem encountered in comparing calculations of structure formation in CDM models to observation is that simulations predict a large overabundance of small halos near galaxies such as our own. Structure formation in these models occurs through hierarchical growth of fragments into larger objects. This hierarchical structure is obvious in clusters of galaxies, where the numerous constituent galaxies are seen directly. Individual galaxy formation is also hierarchical in CDM simulations. These simulations predict a large number of dark matter subhalos, about 500, for each Milky Way–type halo (Moore et al. 1999; Ghigna et al. 2000); however, only 11 dwarf galaxies are observed near our Galaxy. The observed paucity of such substructure (dwarf galaxies) has been interpreted as a fundamental failure of CDM models. The hallmark of *cold* dark matter particles is a very small collisionless damping (free streaming) scale, i.e., considerably smaller than the scale associated with dwarf galaxies, ~ 0.3 Mpc ($\sim 10^{10}\ M_\odot$). Between the large free-streaming scale "top-down" hot dark matter (HDM) structure formation scenarios and the "bottom-up" scenarios of CDM models lies the intermediate regime of WDM (Colombi, Dodelson, & Widrow 1996; Bode et al. 2001), with typical dark matter particles of rest mass ~ 1 keV.

[1] Department of Physics and Center for Astrophysics and Space Sciences, University of California, San Diego, La Jolla, CA 92093-0319.
[2] Harvard-Smithsonian Center for Astrophysics, 60 Garden Street, Cambridge, MA 02138.

On the other hand, the lack of dwarf galaxies may be caused by feedback processes from supernovae and heating in small halos because of the initial formation of very massive stars in a zero-metallicity environment (Bullock, Kravtsov, & Weinberg 2001; Binney, Gerhard, & Silk 2001; Abel et al. 1998). However, it is not clear that these processes would be successful in disrupting dwarf galaxy formation. Nevertheless, there remain many mysteries regarding the earliest stars. Observations of abundances in ultra–metal-poor halo stars may be giving us some new insights into these issues. For example, Qian & Wasserburg (2001) have argued that an inferred increase in [Fe/H] with no concomitant increase in *r*-process abundances may signal the activity of very massive objects.

Another potential problem in CDM models is that the universal density profiles predicted in simulations of structure formation have a monotonic increase of density toward the center of halos. This could give a central "cusp," that is, a discontinuity in the derivative of the spatial density distribution that is a result of the initial singularity in velocity dispersion. The observational searches for a centrally peaked dark matter profile are as yet inconclusive (Swaters, Madore, & Trewhella 2000; van den Bosch et al. 2000). However, the measurement of the innermost rotation curve in dark matter–dominated galaxies may provide the dark matter profile of these halos.

One proposed solution to the central density problem is self-interacting dark matter (Spergel & Steinhardt 2000), which has strong interaction strength forces among dark matter particles and essentially no interactions between dark matter particles and ordinary matter. This kind of interaction would soften cores as a result of efficient energy exchange in halo centers.

In fact, however, Dalcanton & Hogan (2001) find that the core phase-space density distributions in dwarf galaxies and clusters may behave as simple power laws over 8 orders of magnitude in phase density. They argue that such density profiles could not arise from either a WDM or self-interacting dark matter scenario (see also Sellwood 2000).

The idea of using discrete UV photon sources to place limits on the radiative decay of active neutrino HDM was first proposed by Shipman & Cowsik (1981). The lack of UV photons from the rich cluster A665 was used by Melott et al. (1994) to constrain a decaying neutrino dark matter model proposed by Sciama (1990). Our approach to the detection of a radiative flux from cluster cores is similar: we explore the efficacy of X-ray observations in obtaining detections of or constraints on singlet neutrino, active neutrino, and gravitino dark matter candidates.

If observations fail to find the decay flux predicted for a specific dark matter candidate, then the decay constraints presented here can provide upper mass bounds on dark matter candidates. Together with existing structure-derived lower limits on the dark matter particle rest mass in these models, we can potentially exclude specific particle dark matter candidates.

For example, from observation of the power spectrum of the Lyα forest clouds at high redshift, it can be concluded that there is significant structure on small scales. This requires a small collisionless damping scale associated with a dark matter particle with a thermal energy spectrum, and in this limit the particle's rest mass must be greater than 750 eV for a standard warm dark matter particle that decoupled at high temperature (Narayanan et al. 2000). In addition, a paucity of power on small scales can delay the formation of structure at high redshifts and delay cosmological reionization. Such considerations corroborate the Lyα forest constraints and also favor a WDM particle to have a rest mass greater than 750 eV (Barkana, Haiman, & Ostriker 2001). The energy distribution for singlet neutrino relics is different from dark matter that has decoupled at high temperature and is generally "warmer." Colombi et al. (1996) find that the power spectrum for a sterile neutrino with rest mass m_s is the same for a standard WDM relic particle with rest mass m_X if $m_s \approx 2.6 m_X$. Therefore, current lower limits on singlet WDM particle rest mass favor singlet neutrinos with masses $m_s \gtrsim 2.0$ keV.

In § 2, we outline the radiative decay rates that can be probed in deep X-ray observations. Section 3 describes the singlet neutrino, active neutrino, and gravitino WDM candidates and their radiative decay modes. In § 4, we describe specific limits from field galaxy dark matter halos and those from clusters of galaxies. Section 5 presents current diffuse limits on singlet neutrino dark matter. In § 6, we present our conclusions.

2. DARK MATTER HALOS AS PARTICLE RESERVOIRS

An object such as a field galaxy or dwarf galaxy or a cluster of galaxies possessing a dark matter halo of mass $M_{\rm DM}$ will be composed of $N = M_{\rm DM}/m_X$ dark matter particles of rest mass m_X. If Γ_γ is the dark matter particle decay rate into photons of energy E_γ, then the total associated X-ray luminosity is

$$\mathscr{L} \approx \frac{E_\gamma}{m_X} M_{\rm DM} \Gamma_\gamma \, . \tag{1}$$

Here we have assumed that the halo is relatively nearby and that redshift effects on the luminosity are negligible.

For illustration let us take the case where $E_\gamma = m_X/2$ (here, and unless mentioned otherwise, we adopt units where $\hbar = c = 1$). The flux from an object is simply $F = \mathscr{L}/4\pi D_L^2$, where D_L is the luminosity distance to the object. With a reasonable integration time observation of a dark matter halo, a line of energy $E_\gamma = m_X/2$ can be detected at a flux above, for example, $F_{\rm det} = 10^{-13}$ ergs cm^{-2} s^{-1}. (We will show that this actually is the appropriate limit for *Chandra*.) This can place a limit on the radiative decay rate of the relic dark matter particle at

$$\Gamma_\gamma \lesssim (2.4 \times 10^{20} \text{ yr})^{-1} \left(\frac{F_{\rm det}}{10^{-13} \text{ ergs cm}^{-2} \text{ s}^{-1}} \right) \times \left(\frac{M_{\rm DM}^{\rm fov}}{10^{11} \, M_\odot} \right)^{-1} \left(\frac{D_L}{1 \text{ Mpc}} \right)^2 , \tag{2}$$

where $M_{\rm DM}^{\rm fov}$ is the total mass of dark matter within the observed field of view. As we show below, a decay rate limit of this magnitude can be significant in constraining singlet neutrino, active neutrino, and gravitino WDM candidate parameters.

3. WARM DARK MATTER PARTICLE CANDIDATES

3.1. *Singlet Neutrinos*

In general, the neutrino mass eigenstates ν_a ($a = 1, 2, \ldots$) are related by a unitary transformation to the flavor eigenstates ν_α ($\alpha = e, \mu, \tau, s, \ldots$):

$$\nu_a = \sum_\alpha U_{a\alpha} \nu_\alpha \, . \tag{3}$$

A singlet or "sterile" neutrino, ν_s, that has a very small mixing, $\sin^2 2\theta \approx 4|U_{1s}U_{2s}|^2 \ll 1$, with one or more doublet ("active") neutrinos, could be produced nonthermally via active neutrino scattering in the early universe. This was proposed as a WDM candidate by Dodelson & Widrow (1994). Singlet neutrino dark matter also could be produced by matter enhancement (a Mikheyev-Smirnov-Wolfenstein [MSW] resonance; Mikheyev & Smirnov 1985; Wolfenstein 1978) driven by a primordial net lepton number residing in the active neutrino seas (Shi & Fuller 1999). Interestingly, the singlet neutrino could be produced in the requisite numbers to be a WDM candidate in these scenarios even for extremely small vacuum mixing angles, $10^{-13} \lesssim \sin^2 2\theta \lesssim 10^{-7}$.

Supernova constraints on these scenarios were considered by G. M. Fuller.[3] Dolgov & Hansen (2000) did another calculation of the Dodelson & Widrow nonresonant scattering production scenario for WDM singlets and also discussed diffuse photon background and SN 1987A limits on these models.

Singlets with rest mass $m_s \gtrsim 1$ keV are produced during or prior to the quark-hadron transition. In this case, the effects of dilution, enhanced scattering rates, and the evolution of the thermal potential become important. Abazajian, Fuller, & Patel (2001; hereafter AFP) considered singlet WDM production in both the nonresonant Dodelson & Widrow and resonant Shi & Fuller modes and explicitly took account of these early universe thermodynamic effects. AFP also considered in detail constraints on these models arising from diffuse photon backgrounds, cosmic microwave background, ^{6}Li and ^{2}H, big bang nucleosynthesis, and supernova effects limits.

In these models the singlet neutrino is produced in the early universe through nonequilibrium scattering processes involving active neutrinos and other weakly interacting particles. (Singlet neutrinos could be produced via coherent MSW resonance in one limit of matter-enhancement scenarios.) In the matter-enhanced, resonant singlet neutrino production scenarios, the relic density and energy spectrum of the singlet neutrinos can depend on the initial neutrino lepton number residing in the active neutrino seas:

$$L_{\nu_\alpha} \equiv \frac{n_{\nu_\alpha} - n_{\bar{\nu}_\alpha}}{n_\gamma}, \tag{4}$$

where $n_{\nu_\alpha}(n_{\bar{\nu}_\alpha})$ is the neutrino (antineutrino) number density and $n_\gamma = 2\zeta(3)T^3/\pi^2 \approx 0.243T^3$ is the photon number density. In the case of small initial neutrino lepton number ("small" here means the same order of magnitude or smaller than the baryon-to-photon ratio $\eta \sim 10^{-10}$), $L_{\nu_\alpha} \approx 0$, the production occurs at larger mixing angles than in the nonstandard yet plausible case of a large lepton number, $0.001 \lesssim L_{\nu_\alpha} \lesssim 1$. For large lepton numbers, production is resonantly enhanced at low energies, and the energy spectrum of the singlet neutrinos can be "cooler" (that is, possess a smaller collisionless damping scale) than for the case of a thermal energy spectrum (Shi & Fuller 1999).

For the $L_{\nu_\alpha} \approx 0$ case, the fraction of the closure density in singlet neutrinos that is produced in the early universe was found by AFP to be approximately

$$\Omega_{\nu_s} h^2 \approx 0.3\left(\frac{\sin^2 2\theta}{10^{-10}}\right)\left(\frac{m_s}{100\ \mathrm{keV}}\right)^2. \tag{5}$$

Here θ is the vacuum mixing angle defined by an *effective* two-by-two unitary transformation between active ν_α species and a singlet species ν_s:

$$|\nu_\alpha\rangle = \cos\theta|\nu_1\rangle + \sin\theta|\nu_2\rangle,$$
$$|\nu_s\rangle = -\sin\theta|\nu_1\rangle + \cos\theta|\nu_2\rangle, \tag{6}$$

where $|\nu_1\rangle$ and $|\nu_2\rangle$ represent neutrino energy (mass) eigenstates corresponding to vacuum mass eigenvalues m_1 and m_2, respectively. Here we define $h = H_0/(100\ \mathrm{km\ s^{-1}\ Mpc^{-1}})$, where H_0 is the Hubble parameter at the current epoch. It should be kept in mind that future calculations with more sophisticated treatments of the singlet neutrino production physics and the early universe environment may sharpen up, shift, or possibly extend the mass/mixing parameter range that gives interesting relic dark matter contributions.

For nonnegligible lepton numbers, the singlet closure fraction produced depends on the precise value of L_{ν_α} as well as the mixing angle and mass of the singlet neutrino. In general, the matter-enhanced ($L_{\nu_\alpha} \neq 0$) singlet neutrino production modes can produce the same closure fraction as the $L_{\nu_\alpha} \approx 0$ models but do so with orders of magnitude smaller vacuum mixing angles (Shi & Fuller 1999; AFP). As a result, it is in general harder to constrain the $L_{\nu_\alpha} \neq 0$ singlet neutrino production mode scenarios.

Significant constraints can be made on massive neutrinos via the effects of their decay (Dicus, Kolb, & Teplitz 1978). The primary decay channel of massive singlet neutrinos is into three light active neutrinos and is shown in Figure 1. The decay rate corresponding to this process is (Barger, Phillips, & Sarkar 1995; Boehm & Vogel 1987)

$$\Gamma_{3\nu} \approx \sin^2 2\theta G_F^2\left(\frac{m_s^5}{768\pi^3}\right)$$
$$\approx 8.7 \times 10^{-31}\ \mathrm{s^{-1}}\left(\frac{\sin^2 2\theta}{10^{-10}}\right)\left(\frac{m_s}{1\ \mathrm{keV}}\right)^5, \tag{7}$$

where $G_F \approx 1.166 \times 10^{-11}\ \mathrm{MeV^{-2}}$ is the Fermi constant. This process needs to be considered when comparing number densities of singlets produced at a very early time with those today, for example, in the calculation of the diffuse extragalactic background radiation (see § 5).

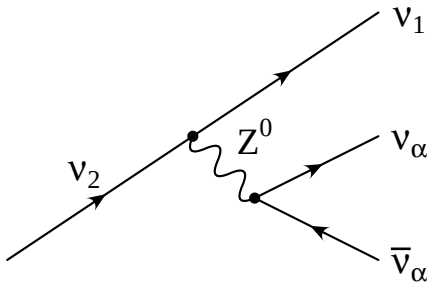

FIG. 1.—Principal decay mode for massive singlet neutrinos with mass less than twice the electron mass. There are three light active neutrinos in the final state. (Here, $\alpha = e$, μ, and τ.)

[3] Fuller, G. M. 2000, Neutrino Astrophysics and Cosmology (lectures at the XXVIII SLAC Summer Institute on Particle Physics: Neutrinos from the Lab, the Sun, and the Cosmos). Available at http://www.slac.stanford.edu/gen/meeting/ssi/2000/fuller.html.

The principal radiative decay modes of singlet neutrinos are shown in Figure 2. Majorana neutrinos have contributions from conjugate processes. For the Majorana neutrino case, the decay rate for $m_2 \gg m_1$ is (Pal & Wolfenstein 1982)

$$\Gamma_\gamma = \frac{\alpha G_F^2}{64\pi^4} m_2^5 \left[\sum_\beta U_{1\beta} U_{2\beta} F(r_\beta) \right]^2 , \quad (8)$$

where $\alpha \approx 1/137$ is the fine-structure constant. Here, $r_\beta = (m_\beta/M_W)^2$ is the square of the ratio of the β flavor charged lepton mass and the $W^\pm$ boson mass, and

$$F(r_\beta) \approx -\tfrac{3}{2} + \tfrac{3}{4} r_\beta . \quad (9)$$

The sum in equation (8) is over the charged lepton flavors. For decay of a doublet neutrino into another flavor doublet, the sum in equation (8) vanishes for the first term in equation (9) on account of the unitarity property associated with the transformation matrix elements in equation (3). The second term in equation (9) causes the sum not to vanish, but the resulting term is obviously very small because it involves the fourth power of the ratio of charged lepton to $W^\pm$ masses. This is the so-called Glashow-Iliopoulos-Maiani (GIM) suppression (or cancellation).

For a singlet decay, the sum over the charged lepton flavors in equation (9) does not cancel the leading contribution in equation (9) because there is no charged lepton associated with the singlet state. The decay rate is consequently greatly enhanced over the GIM-suppressed doublet decay case. The rate of singlet neutrino radiative decay is

$$\Gamma_\gamma(m_s, \sin^2 2\theta) \approx 6.8 \times 10^{-33} \text{ s}^{-1} \left(\frac{\sin^2 2\theta}{10^{-10}} \right) \left(\frac{m_s}{1 \text{ keV}} \right)^5 , \quad (10)$$

where we have identified $m_s \approx m_2$, since the mixing is presumed to be small.

The singlet neutrino can also decay via two-photon emission, $\nu_2 \rightarrow \nu_1 + \gamma + \gamma$. However, this decay has a leading contribution scaling with the inverse square of the charged lepton mass (Nieves 1983) and therefore is strongly suppressed. Since the two-photon decay rate scales as m_s^9, it will dominate over the single-photon mode for masses $m_s \gtrsim 10$ MeV. However, singlet neutrino masses over 10 MeV are excluded by other considerations (AFP).

In the case of the single-photon channel, the decay of a nonrelativistic singlet neutrino into two (nearly) massless particles produces a line at energy $E_\gamma = m_s/2$ with a width given by the velocity dispersion of the dark matter. For example, clusters of galaxies typically have a virial velocity dispersion of ~ 300 km s^{-1}. Therefore, the emitted line is very narrow, $\Delta E \sim 10^{-3} E_\gamma$. The observed width of the line will be given by the energy resolution of the detector in this case. For example, the energy resolution of *Chandra*'s Advanced CCD Imaging Spectrometer (ACIS) is $\Delta E \approx 200$ eV, while the Constellation X project hopes to achieve a resolution of $\Delta E \approx 2$ eV.

The luminosity from a general singlet neutrino dark matter halo is (from eq. [1])

$$\mathscr{L} \approx 6.1 \times 10^{32} \text{ ergs s}^{-1} \left(\frac{M_{DM}}{10^{11} M_\odot} \right) \left(\frac{\sin^2 2\theta}{10^{-10}} \right) \left(\frac{m_s}{1 \text{ keV}} \right)^5 . \quad (11)$$

This implies that the radiative decay flux from singlet neutrinos in the halo is

$$F \approx 5.1 \times 10^{-18} \text{ ergs cm}^{-2} \text{ s}^{-1} \left(\frac{D_L}{1 \text{ Mpc}} \right)^{-2} \times \left(\frac{M_{DM}}{10^{11} M_\odot} \right) \left(\frac{\sin^2 2\theta}{10^{-10}} \right) \left(\frac{m_s}{1 \text{ keV}} \right)^5 . \quad (12)$$

Therefore, for a general singlet neutrino candidate with rest mass m_s and vacuum mixing angle $\sin^2 2\theta$, the mass limit—assuming no detection of a line at a flux limit level of F_{det}—is

$$m_s \lesssim 4.6 \text{ keV} \left(\frac{D_L}{1 \text{ Mpc}} \right)^{2/5} \left(\frac{F_{det}}{10^{-13} \text{ ergs cm}^{-2} \text{ s}^{-1}} \right)^{1/5} \times \left(\frac{M_{DM}}{10^{11} M_\odot} \right)^{-1/5} \left(\frac{\sin^2 2\theta}{10^{-10}} \right)^{-1/5} . \quad (13)$$

Using equation (5), the dependence on mixing angle can be eliminated, and with equation (1), we have for the $L_{\nu_\alpha} \approx 0$ case that the flux due to singlet neutrino decay is

$$F \approx 5.1 \times 10^{-14} \text{ ergs cm}^{-2} \text{ s}^{-1} \left(\frac{D_L}{1 \text{ Mpc}} \right)^{-2} \times \left(\frac{M_{DM}}{10^{11} M_\odot} \right) \left(\frac{\Omega_{\nu_s} h^2}{0.3} \right) \left(\frac{m_s}{1 \text{ keV}} \right)^3 . \quad (14)$$

For the $L_{\nu_\alpha} \approx 0$ production case, the corresponding singlet mass limit from a null detection of a line at $E_\gamma = m_s/2$ at flux limit F_{det} is

$$m_s \lesssim 1.25 \text{ keV} \left(\frac{D_L}{1 \text{ Mpc}} \right)^{2/3} \left(\frac{F_{det}}{10^{-13} \text{ ergs cm}^{-2} \text{ s}^{-1}} \right)^{1/3} \times \left(\frac{M_{DM}}{10^{11} M_\odot} \right)^{-1/3} \left(\frac{\Omega_{\nu_s} h^2}{0.3} \right)^{-1/3} . \quad (15)$$

It should be noted that the decay limits presented here derive from a specific type of mass-generation mechanism

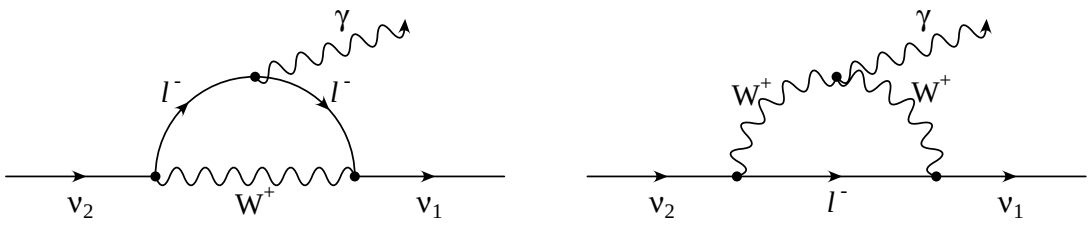

FIG. 2.—Principal radiative decay modes for massive singlet neutrinos

for the singlet neutrino: those arising from the simplest case of Majorana or Dirac-type mass terms. More complicated neutrino mass models would have different mass terms, radiative decay widths, and possibly other couplings, and bounds on these models would require individual analysis.

3.2. *Active Neutrinos*

The direct experimental upper limits on the ν_μ and ν_τ masses are only 190 keV and 18.2 MeV, respectively (Groom et al. 2000). Although the observationally inferred age of the universe precludes the possibility of fully thermalized active neutrinos being the WDM or CDM (Gerstein & Zeldovich 1966; Cowsik & McClelland 1972), the active neutrinos may not be fully thermalized in the early universe if the postinflation reheating temperature is low (Kawasaki, Kohri, & Sugiyama 2000; Giudice, Kolb, & Riotto 2001a). In this case, the ν_μ and/or ν_τ can be legitimate WDM candidates (Giudice et al. 2001b).

The radiative decay rate of massive active neutrinos into a single photon in a three-generation neutrino model is suppressed by the GIM mechanism and is slower than the singlet neutrino decay rate by a factor $(m_\alpha/M_W)^4 \sim 10^{-21}$, and therefore negligible. The two-photon decay mode $\nu_2 \rightarrow \nu_1 + \gamma + \gamma$ for massive active neutrino decay has a GIM suppression factor of $\sim(m_a/m_\alpha)^4$, where m_a is the relevant vacuum neutrino mass eigenvalue and m_α is the mass of the charged lepton of flavor α (Nieves 1983). This rate can therefore dominate the single-photon mode only for $m_a \gtrsim$ 200 keV, which is outside of the range of interest for active neutrino WDM. Therefore, active neutrino WDM in a three-generation neutrino model is relatively stable and robust against decay constraints.

In order to accommodate solar and atmospheric neutrino oscillation solutions to experimental data, a light singlet neutrino with mass $m_s \ll m_{\nu_{\mu,\tau}}$ must be a feature of any neutrino mass/mixing scheme that can provide for an active ν_μ/ν_τ WDM candidate. If there is a light singlet, then the decay from the mass eigenstates most closely associated with the ν_μ/ν_τ doublet into a mass state more closely associated with the lighter singlet is not GIM suppressed. This process can lead to a rapid radiative decay of the active WDM candidate. However, the mixing between the two mass eigenstates can be tuned to be arbitrarily small, since it is not phenomenologically required to be nonzero. If a spectral feature in the X-ray is observed, however, it may indicate a nonnegligible mixing between a massive active neutrino and a lighter singlet neutrino.

3.3. *Gravitinos*

Another WDM candidate is the gravitino, $\tilde{G}$, the spin $\frac{1}{2}$ supersymmetric partner to the graviton (Kawasaki, Sugiyama, & Yanagida 1997). In the minimal supersymmetric standard model, the assumption of R-parity conservation is made, originally motivated by the need to explain the slow proton decay rate. The gravitino can be the lightest supersymmetric particle (LSP) and, with R-parity conservation, it is stable. However, there has been considerable interest in R-parity violation in supersymmetric models as a mechanism for neutrino mass generation (Hall & Suzuki 1984), motivated by the considerable evidence for neutrino mass (for a review, see Caldwell 1998). The gravitino may also be the LSP and the dark matter (Takayama & Yamaguchi 2000) in R-parity–violating models with gauge mediation (Dine et al. 1996) or with a low gravitational scale (or effective Planck scale $M_{\rm Pl}$), which comes about through large extra dimensions (Arkani-Hamed, Dimopoulos, & Dvali 1998).

The gravitino LSP decays with a long lifetime in these models since its decay is suppressed by $M_{\rm Pl}^2$. In one specific example considered by Takayama & Yamaguchi (2000), the R-parity violation is bilinear, with the lightest neutralino being bino-dominant. In this case, the dominant decay mode of the gravitino is $\tilde{G} \rightarrow \gamma\nu$ through a coupling of the gravitino with the photon and its superpartner, the photino, which has a neutrino component. The lifetime of the gravitino is approximately

$$\Gamma_\gamma(\tilde{G} \rightarrow \gamma\nu) \approx \frac{1}{4} |U_{\gamma\nu}|^2 \frac{m_{3/2}^3}{M_{\rm Pl}^2}, \tag{16}$$

where $U_{\gamma\nu}$ represents the neutrino component of the photino and $m_{3/2}$ is the gravitino mass.

In the models accommodating neutrino masses associated with the atmospheric neutrino problem, $U_{\gamma\nu}$ has a characteristic value $|U_{\gamma\nu}|^2 \approx 7 \times 10^{-13}$. The decay rate of the gravitino into photons is then

$$\Gamma_\gamma(\tilde{G} \rightarrow \gamma\nu) \approx (2.6 \times 10^{19}\ \text{yr})^{-1} \left(\frac{m_{3/2}}{1\ \text{GeV}}\right)^3 \times \left(\frac{|U_{\gamma\nu}|^2}{7 \times 10^{-13}}\right) \left(\frac{M_{\rm Pl}}{M_{\rm Pl}^0}\right)^{-2}, \tag{17}$$

where $M_{\rm Pl}^0 \approx 1.22 \times 10^{19}$ GeV is the conventional Planck scale. The decay would produce a photon line at an energy of $E_\gamma \approx m_{3/2}/2$. For a $\sim$1 keV mass gravitino, the decay rate is far below the detectable limit given by equation (2). However, as mentioned previously, the gravitino is the LSP in some supersymmetric models with large extra dimensions. These scenarios generically reduce the effective Planck scale by up to 14 orders of magnitude. From equation (17), if the effective Planck scale is reduced by "only" 7 orders of magnitude, the rate becomes detectable. Ultimately, the lack or presence of a photon emission line may constrain supersymmetric dark matter models with large extra dimensions.

4. OBSERVING DARK MATTER HALOS

Astronomical objects with strong evidence for dark matter concentrations can serve as source reservoirs for WDM particles. The specific amount of dark matter in the observed region can be inferred from models of the spatial distribution of the dark matter. The theoretical basis for the dark matter distribution is based on either local or cosmological physics.

Local models include truncated isothermal sphere configurations, which describe galactic dark matter halos as perfect gases in equilibrium. The isothermal sphere model reproduces well the observed flat rotation curves of spiral galaxies. In another local-type model, the dark matter in X-ray clusters of galaxies is assumed to be the dominant source of the gravitational potential binding the hot X-ray–emitting intracluster medium in hydrostatic equilibrium in the β-model.

In CDM models, both galaxy and galaxy cluster halos can be the result of hierarchical clustering and so can possess a unified profile. However, CDM models and their corresponding unified profiles may be too centrally concentrated to describe dwarf galaxy rotation curves (Navarro,

Frenk, & White 1995, 1996). The general dark matter density profile with radius $\rho(r)$ for hierarchical clustering is dubbed the Navarro-Frenk-White (NFW) profile:

$$\rho(r) \propto \left(\frac{r}{r_s}\right)^{-1}\left(1+\frac{r}{r_s}\right)^{-2}, \quad (18)$$

where r_s is the scale radius.

Given any dark matter distribution for an object, the photon flux resulting from particle decay or interaction is simply proportional to the mass within the field of view. This can be approximated as the mass within the projected radius at the distance of the object. However, the dark matter in the field of view contains not only the extended halo out to the projected radius but also the material in front of and behind this sphere. To determine the mass within the rectangular prism cut out of the extended halo of the object, we have performed a Monte Carlo integration of the region's mass density, sampling according to an assumed density profile, e.g., NFW.

4.1. *Instrumental Background*

For low surface brightness dark matter systems, the primary limit to dark matter flux detection is instrumental background. In particular, ACIS aboard *Chandra* has a background of 2×10^{-2} counts s^{-1} in a $\sim$200 eV energy bin of the imaging array.

As a rough approximation, we can estimate the flux onto ACIS from dark matter decay requisite to produce a 4 σ detection. For a line with flux $F_{-14} \equiv F/(10^{-14}$ ergs cm^{-2} s$^{-1})$, the count rate is $C_L \approx 3 \times 10^{-4} F_{-14}$ counts s^{-1}. For an observation of integration time $t_5 \equiv t/(10^5$ s), the background is $B \approx 2 \times 10^3 t_5$ counts. The count level required to overcome the background at 4 σ is

$$C_L \approx \frac{4\sqrt{B}}{t}. \quad (19)$$

Therefore, the detectable flux is

$$F_{-14}^{\rm det} \approx 6 t_5^{-1/2}. \quad (20)$$

For low surface brightness sources, an observation with an integration time of 36,000 s ($t_5 = 0.36$) can detect a flux $\approx 10^{-13}$ ergs cm^{-2} s^{-1} ($F_{-14}^{\rm det} = 10$). One must modify the estimated detectable WDM flux whenever the baryon-associated material (e.g., electrons, protons, iron, etc.) in these halos provides an ambient X-ray flux in excess of 3×10^{-11} ergs cm^{-2} s^{-1}. In such circumstances the minimum detectable WDM flux in a $\sim$200 eV energy bin, corresponding to the ACIS energy resolution, is

$$F_{-14}^{\rm det} \approx 6\left(\frac{F_{\rm source}}{3 \times 10^{-11}}\right)^{1/2} t_5^{-1/2} \text{ ergs cm}^{-2} \text{ s}^{-1}. \quad (21)$$

In Figure 3 we show contours of WDM X-ray photon decay flux in lines at photon energies $E_\gamma = m_s/2$ as a function of the dark matter mass in the field of view modulo its luminosity distance (see eq. [14]) for a WDM singlet neutrino model with zero initial lepton number, $L_{\nu_\alpha} \approx 0$. This figure provides a shaded region indicating detectability with ACIS on *Chandra* for a 36 ks observation.

4.2. *Clusters of Galaxies*

Clusters of galaxies are massive objects ($\sim 10^{15} M_\odot$), and there is strong evidence that most of this mass is carried by dark matter. Mass estimates are derived from a spherical hydrostatic equilibrium model that assumes that the gas in the intracluster medium is solely supported by thermal pressure. The enclosed mass at a radius r is given by

$$M(<r) = -\frac{kT_{\rm X}(r)}{G\mu m_p} r\left[\frac{d\log \rho_g(r)}{d\log r} + \frac{d\log T_{\rm X}(r)}{d\log r}\right], \quad (22)$$

where $G = (M_{\rm Pl}^0)^{-2}$, μm_p is the average molecular weight of the gas (m_p is the proton mass), k is Boltzmann's constant, $\rho_g(r)$ is the gas density profile, and $T_{\rm X}(r)$ is the temperature profile. Using this equilibrium model, an approximate isothermal fit to the mass profile can be made. This is the so-called isothermal β-model. The enclosed mass for the isothermal β-model is

$$M(<r) \approx 1.13 \times 10^{14} M_\odot \left(\frac{T_{\rm X}}{\rm keV}\right)\left(\frac{r}{\rm Mpc}\right)\frac{(r/r_c)^2}{1+(r/r_c)^2}, \quad (23)$$

where r_c is the core radius (Cavaliere & Fusco-Femiano 1978). (Note that r_c and r_s are related but not identical.)

With contemporary X-ray telescopes (*ASCA*, *XMM-Newton*, and *Chandra*) able to provide spatially resolved temperature profiles, the hydrostatic equilibrium β-model in principle can yield accurate mass estimates. However, as yet, detailed analyses along these lines to provide $T_{\rm X}(r)$ are still being done. Therefore, we employ the isothermal β-model with average temperature values. These are available for the 24 clusters that we consider.

In this work we use the average temperatures of rich clusters from the Horner, Mushotzky, & Scharf (1999) database. Redshifts or distances are taken from the SIMBAD database.[4] The physical properties of the clusters that we consider are given in Table 1.

We can approximate the reservoir of dark matter mass and observable decay flux for singlet neutrino dark matter seen by ACIS aboard the *Chandra* observatory using the relation between the projected radius of the field of view, $R_{\rm fov}$, and the angular field of view of ACIS, $\theta_{\rm fov} \approx 5 \times 10^{-3}$ rad: $D_L = 2R_{\rm fov}/\theta_{\rm fov} \approx 4 \times 10^2 R_{\rm fov}$. With equation (14), for the $L_{\nu_\alpha} \approx 0$ case, the expected X-ray flux is then

$$F \approx 3 \times 10^{-19} \text{ ergs cm}^{-2} \text{ s}^{-1}\left(\frac{m_s}{\rm keV}\right)^3\left(\frac{\Omega_{\nu_s} h^2}{0.3}\right) \times \left(\frac{M_{\rm DM}}{10^{11} M_\odot}\right)\left(\frac{R_{\rm fov}}{1 \text{ Mpc}}\right)^{-2}. \quad (24)$$

The core radius falls within the field of view of *Chandra* for all clusters that we consider except for the Coma Cluster. Since the mass increases approximately with the radius outside of the core, we can approximate $M_{\rm fov} \sim M_{\rm core} R_{\rm fov}/r_c$. Therefore, the expected X-ray flux from the cluster in the $L_{\nu_\alpha} \approx 0$ model is

$$\begin{aligned} F &\approx 3 \times 10^{-19} \text{ ergs cm}^{-2} \text{ s}^{-1}\left(\frac{m_s}{\rm keV}\right)^3\left(\frac{M_{\rm core}}{10^{11} M_\odot}\right) \times \left(\frac{r_c}{1 \text{ Mpc}}\right)^{-1}\left(\frac{R_{\rm fov}}{1 \text{ Mpc}}\right)^{-1} \\ &\approx 1.2 \times 10^{-16} \text{ ergs cm}^{-2} \text{ s}^{-1}\left(\frac{m_s}{\rm keV}\right)^3 \times \left(\frac{M_{\rm core}}{10^{11} M_\odot}\right)\left(\frac{D_L}{1 \text{ Mpc}}\right)^{-1}\left(\frac{R_{\rm fov}}{1 \text{ Mpc}}\right)^{-1}. \end{aligned} \quad (25)$$

[4] Available at http://simbad.u-strasbg.fr.

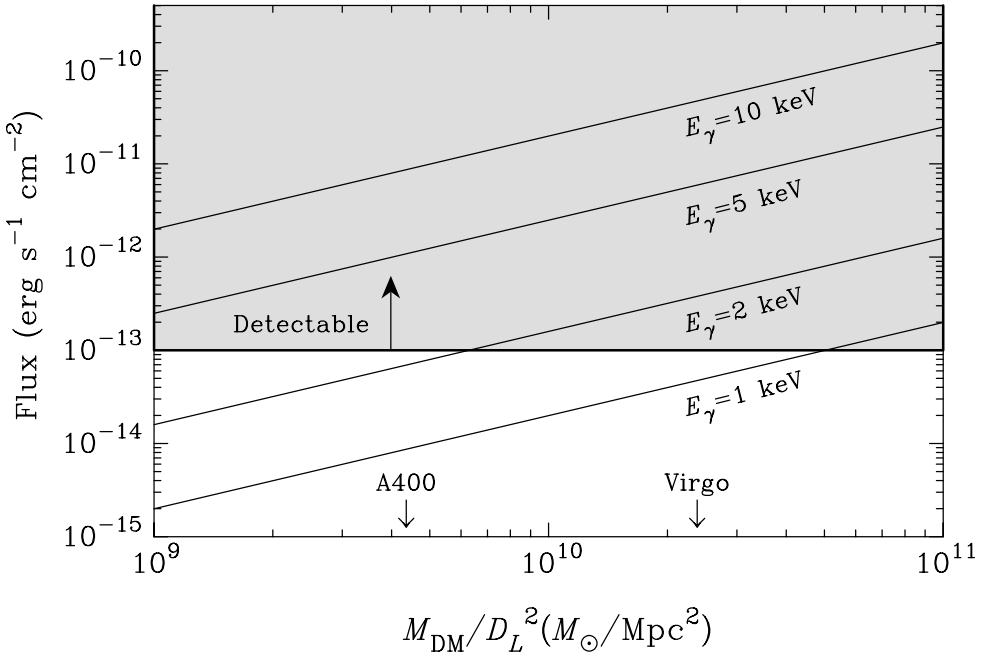

FIG. 3.—Singlet neutrino decay X-ray flux produced by an object with a mass M_{DM} at distance D_L. Shown are contours that correspond to spectral lines with energy E_γ produced by singlet neutrinos of mass $m_s = 2E_\gamma$. The shaded region indicates detectability with ACIS on *Chandra* for a 36 ks observation.

In order to more accurately determine the dark matter mass and luminosity in decay photons, we estimate the dark matter mass within the rectangular prism cut out of the spherical isothermal β-model density distribution in the dark matter halo. The prism has the dimensions of $2R_{fov} \times 2R_{fov} \times 2R_{vir}$, where R_{fov} is half the projected size of the aperture, $R_{fov} \approx \theta_{fov} D_L/2$, and where R_{vir} is the cluster's virial radius. We use a Monte Carlo integration to find the

TABLE 1

CLUSTERS OF GALAXIES

Name	$M_{vir}(M_X)$[a] ($\times 10^{14}\ h^{-1}\ M_\odot$)	r_c[a] (h^{-1} Mpc)	M_{core}[b] ($\times 10^{14}\ M_\odot$)	M_{DM}^{fov}[c] ($\times 10^{14}\ M_\odot$)	Γ_γ Limit[d] (yr^{-1})	$m_s(L_{\nu_\alpha} \approx 0)$ Limit[e] (keV)
2A0335+096.....	(1.10)	0.023	0.036	1.04	$(1.1 \times 10^{19})^{-1}$	4.5
A0085.....	9.88	0.086	0.313	3.53	$(1.6 \times 10^{19})^{-1}$	3.9
A0119.....	2.50	0.231	0.312	2.23	$(1.4 \times 10^{19})^{-1}$	4.1
A0262.....	1.32	0.032	0.029	0.33	$(1.6 \times 10^{19})^{-1}$	3.9
A0400.....	2.49	0.051	0.076	0.47	$(1.0 \times 10^{19})^{-1}$	4.5
A0426.....	9.08	0.020	0.063	1.08	$(4.3 \times 10^{19})^{-1}$	2.8
A0496.....	3.20	0.035	0.058	1.40	$(1.6 \times 10^{19})^{-1}$	3.9
A0539.....	2.01	0.082	0.094	1.00	$(1.6 \times 10^{19})^{-1}$	4.0
A1060.....	1.90	0.040	0.045	0.38	$(3.7 \times 10^{19})^{-1}$	2.9
A1656.....	4.97	0.208	0.245	1.98	$(4.7 \times 10^{19})^{-1}$	2.7
A1795.....	5.86	0.068	0.171	4.20	$(1.3 \times 10^{19})^{-1}$	4.2
A2063.....	3.04	0.067	0.110	1.43	$(1.4 \times 10^{19})^{-1}$	4.1
A2199.....	5.71	0.040	0.102	1.42	$(2.0 \times 10^{19})^{-1}$	3.6
A2256.....	23.12	0.228	1.40	5.26	$(1.8 \times 10^{19})^{-1}$	3.8
A2319.....	39.54	0.135	1.24	4.87	$(1.9 \times 10^{19})^{-1}$	3.7
A2634.....	4.31	0.123	0.273	0.98	$(1.3 \times 10^{19})^{-1}$	4.2
A3526.....	(0.80)	0.038	0.043	0.37	$(3.9 \times 10^{19})^{-1}$	2.9
A3558.....	11.54	0.075	0.318	2.22	$(1.2 \times 10^{19})^{-1}$	4.3
A3571.....	8.17	0.086	0.241	2.95	$(2.3 \times 10^{19})^{-1}$	3.5
A4059.....	(1.50)	0.075	0.164	1.73	$(1.0 \times 10^{19})^{-1}$	4.6
AWM 7	5.77	0.062	0.148	0.65	$(2.8 \times 10^{19})^{-1}$	3.3
MKW 3S.....	(2.00)	0.047	0.067	1.83	$(1.2 \times 10^{19})^{-1}$	4.3
MKW 4	1.15	0.009	0.0070	0.30	$(9.7 \times 10^{18})^{-1}$	4.6
Virgo	2.04	0.007	0.0081	0.10	$(5.6 \times 10^{19})^{-1}$	2.6

[a] The values of M_{vir} and r_c are from Horner et al. 1999. For clusters whose M_{vir} is not well known, we used the mass determined by the X-ray profile, M_X (shown in parentheses).

[b] The mass within the core radius M_{core}.

[c] The mass within the field of view M_{DM}^{fov} (density integrated over the rectangular prism in the field of view).

[d] The potential limit on the radiative decay rate Γ_γ of dark matter from the object with a 36 ks observation.

[e] The corresponding constraint on the singlet neutrino mass, m_s, in the $L_{\nu_\alpha} \approx 0$ case (eq. [15]).

dark matter mass within this field of view, which can be significantly larger than the mass strictly within the spherical volume defined by the core radius.

We can use equation (15) to provide a rough limit on the mass m_s of a singlet neutrino candidate assumed to comprise the dark matter halo. The limits on m_s for various clusters are given in Table 1. The best limit, $m_s \lesssim 2.6$ keV (for the $L_{\nu_\alpha} \approx 0$ case), is provided by the Virgo Cluster.

In Figure 4 we give contours in singlet mass m_s and vacuum mixing angle space of singlet neutrino closure fraction $\Omega_s \approx 0.3$ (for $h = 0.7$) for three values of primordial lepton number ($L \equiv L_{\nu_\alpha}$): $L \approx 0$, $L \approx 0.01$, and $L \approx 0.1$. The nonzero lepton number contours are very rough fits to the results of AFP. (Note that lepton number L here is denoted as $\mathscr{L}$ in AFP.) Superimposed on this figure are shaded regions indicating potential detectability or exclusion of singlet neutrino WDM from *Chandra* observations of the Virgo Cluster for a 36 ks observation (*dark shade bounded by the solid line*) and a 100 ks observation (*bounded by the dashed line*). The *Chandra* observations of the Virgo Cluster can come close to eliminating all of the $L \approx 0$, nonresonant singlet production mode case. In the next section, we will argue that the Constellation X project can give even broader constraints in this figure.

To study the possible observational signature of a singlet neutrino halo in the Virgo Cluster, we generate spectra of the gas in Virgo as seen with ACIS with WEBSPEC (XSPEC). We use the MEKAL model for the X-ray flux for the gas at a temperature of 2.54 keV (Horner et al. 1999) with a thermal X-ray flux from the central region of 1.5×10^{-12} ergs cm^{-2} s^{-1} in the 2–10 keV band (Böhringer et al. 2001). We adopt a distance to the Virgo cluster of 20.7 Mpc measured from 21 cm line widths by Federspiel, Tammann, & Sandage (1998).

In Figure 5, we show the binned spectrum for two cases. We include the decay fluxes (see eq. [14]) from a singlet neutrino halo composed of 4 and 5 keV singlet neutrinos producing decay photons of energy 2 and 2.5 keV, respectively, for a 50 ks observation on *Chandra*'s ACIS. In addition, we include the theoretical MEKAL model gas emission spectrum. The residuals from this standard gas emission prediction are given at the bottom of the figure. The width of the lines is nearly entirely due to instrumental broadening.

From this unsophisticated example, it is obvious that a line feature produced by a 5 keV singlet neutrino would be readily detectable, while the detection/elimination of the decay line for a 4 keV singlet would require a statistical analysis. With the lack of such a strong line anomaly in the observation of M87 in the core of the Virgo Cluster with *XMM-Newton* by Böhringer et al. (2001), we can conclude that the dark matter in the Virgo Cluster is not composed of singlet neutrinos with masses $m_s \gtrsim 5$ keV created in the early universe with $L_{\nu_\alpha} \approx 0$. The potential constraints on general L_{ν_α} scenarios from statistical spectral analyses are shown in Figure 4.

4.3. *Field Spiral Galaxies*

Field galaxies can provide low gas X-ray emission sources for dark matter, but these objects do not represent as concentrated a dark matter source as do clusters of galaxies. A detailed observation of the structure and rotation of NGC 4123 has allowed a fit to disk and halo models that places a lower limit on the profile of the dark matter halo

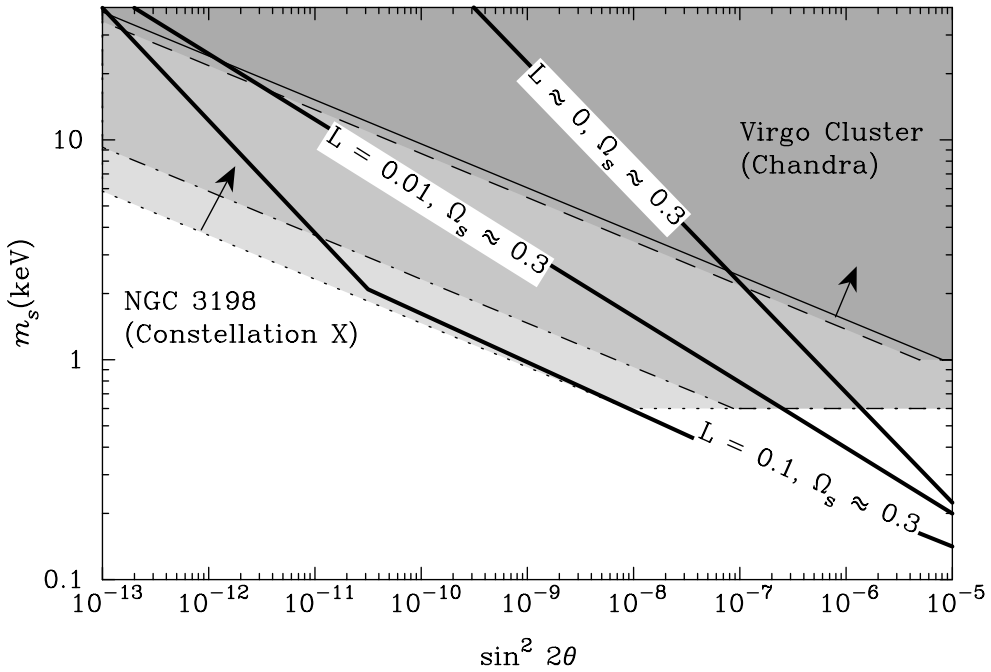

FIG. 4.—Shown are approximate contours for $\Omega_s \approx 0.3$ ($h = 0.7$) for singlet neutrino WDM models with different initial lepton number, L. Potential detection/exclusion of the models can be made in the darkest gray region with a limiting line flux of 10^{-13} ergs cm^{-2} s^{-1} from the Virgo Cluster observed with *Chandra*'s ACIS (from a 36 ks observation). The dashed line is the limit for a 100 ks observation with *Chandra*, also for Virgo. The medium-gray region bounded by the dashed-dotted line indicates the detection/exclusion range for Constellation X observation of field spiral galaxy NGC 3198 for a 1000 ks observation, and the light-gray region indicates the possibility of detection/exclusion for an ambitious 10 Ms observation (presumably obtained in several observations over a few years).

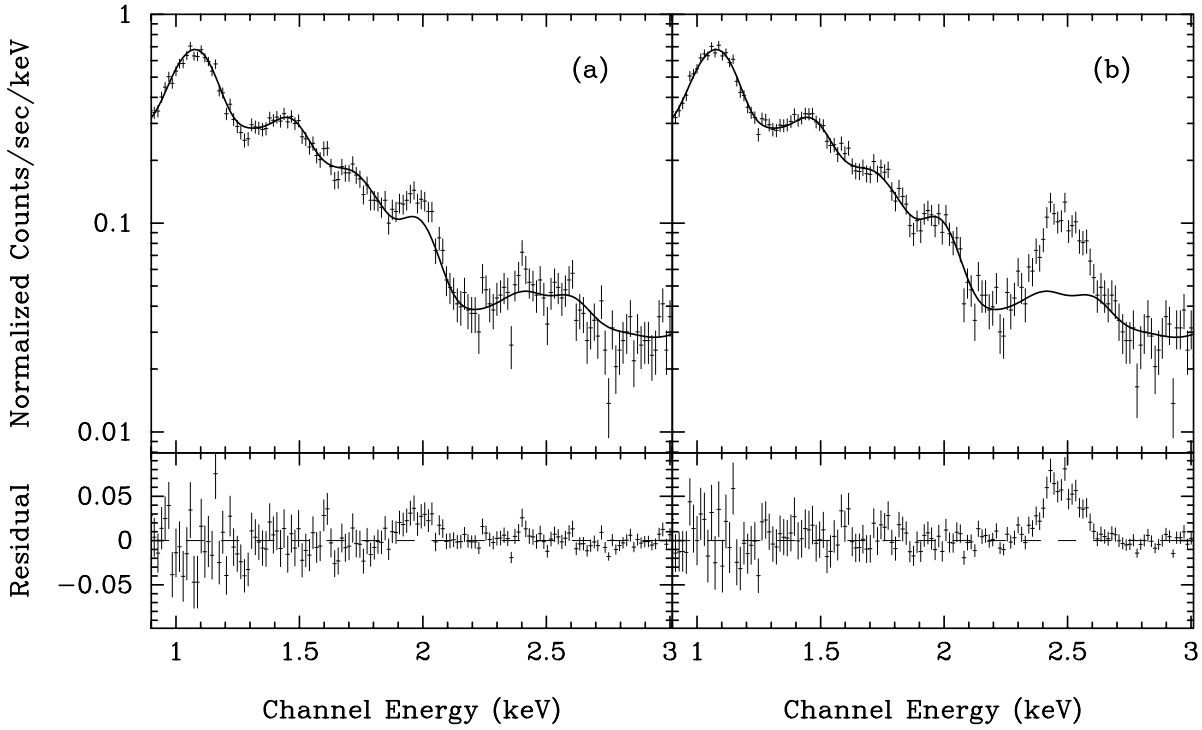

FIG. 5.—Synthesized spectrum viewed by *Chandra*'s ACIS modeling the central region of the Virgo Cluster, for two different cases of singlet neutrino mass, showing a strong mass dependence of the flux in a line at (*a*) a 4 keV singlet neutrino halo (producing a 2 keV line) and (*b*) a 5 keV singlet neutrino halo (producing a 2.5 keV line). Integration time is assumed to be 50 ks, with a $T_X = 2.54$ keV thermal flux (1.5×10^{-12} ergs cm^{-2} s^{-1}) from the gas in Virgo generated with the MEKAL model, which is shown as the solid line. Residuals from the gas emission model alone are shown at the bottom. The width of the line is nearly entirely due to instrumental energy resolution.

(Weiner et al. 2001). Using a maximal disk model to fit the observed rotation curve, they find that a dark halo remains required. We use an NFW-type profile halo fitted by Weiner et al. (2001) and find the resulting lower bound on the dark matter mass in the field of view. The distance to NGC 4123 is approximately 22.4 Mpc. The form of the NFW profile used is the two-parameter spherical density distribution:

$$\rho_{\rm NFW} = \rho_s \frac{4r_s^3}{r(r + r_s)^2} . \tag{26}$$

The halo parameters are from Weiner et al. (2001) and are given in Table 2. The possible limit from a 36 ks exposure (see eq. [15]) is $m_s \lesssim 10.3$ keV in the $L_{\nu_\alpha} \approx 0$ production mode case.

We also use the rotation curve of NGC 3198 (van Albada et al. 1985) to fit an NFW profile for the dark matter in this object. We use a mass-to-light ratio of unity, which provides a good fit for the inner part of the rotation curve. The halo parameters are given in Table 2. We adopt a distance of 18.34 Mpc to NGC 3198, from Willick & Batra (2001). The potential mass limit (eq. [15]) for a 36 ks observation in this case is $m_s \lesssim 6.0$ keV for the $L_{\nu_\alpha} \approx 0$ models.

In Figure 4 we show the detectability region for observations of NGC 3198 with Constellation X—a proposed fleet of observatories that will have an effective area ~ 10 times greater than *Chandra* and no instrumental background (Valinia et al. 1999)—for two integration times, 1 and 10 Ms, which conceivably could be achieved through several long observations over a few years. An exposure equivalent to this could be obtained by a stacking analysis of the spectra of a number of similar clusters (see, e.g., Brandt et al. 2001; Tozzi et al. 2001). Constellation X, with very long integration times, holds out the prospect of covering nearly the entire WDM parameter space of interest for

TABLE 2

FIELD GALAXIES

Name	ρ_s ($\times 10^{14}\ M_\odot$ Mpc^{-3})	r_s (kpc)	$M(<r_s)$ ($\times 10^{11}\ M_\odot$)	$M_{\rm DM}^{\rm fov}$ [a] ($\times 10^{11}\ M_\odot$)	Γ Limit[b] (yr^{-1})	$m_s(L_{\nu_\alpha} \approx 0)$ Limit[c] (keV)
NGC 3198.....	1.5	67.0	4.32	3.62	$(2.3 \times 10^{18})^{-1}$	6.0
NGC 4123.....	1.3	38.2	0.704	1.85	$(2.3 \times 10^{17})^{-1}$	10.3

[a] The mass within the field of view $M_{\rm DM}^{\rm fov}$ (density integrated over the rectangular prism in the field of view).
[b] The potential limit on the radiative decay rate Γ_γ of dark matter from the object with a 36 ks observation.
[c] The corresponding constraint on the singlet neutrino mass, m_s, in the $L_{\nu_\alpha} \approx 0$ case (eq. [15]).

some of the resonant production mode scenarios up to lepton number $L \lesssim 0.1$.

We should note, however, that it is still uncertain how low in m_s (i.e., X-ray photon line energy) Constellation X can be sensitive to at the limiting X-ray flux given in Figure 4 (10^{-19} ergs cm^{-2} s^{-1}). In fact, it could be that the lowest photon energy detectable on Constellation X could be between 0.3 and 0.5 keV. We show the possible constraint with detectability down to 0.3 keV photons, or $m_s \approx 0.6$ keV. As described in the introduction, Lyα forest considerations disfavor $m_s \lesssim 2.0$ keV, and therefore Constellation X in principle can detect/exclude essentially all of the remaining singlet neutrino parameter space for $L_{\nu_\alpha} \lesssim 0.1$.

5. DIFFUSE PHOTON LIMITS

The flux per unit energy per unit solid angle from a homogeneously distributed decaying background dark matter particle is (Massó & Toldrà 1999)

$$\frac{d^2F}{dE_\gamma\, d\Omega} = \frac{\Gamma_\gamma}{4\pi}\frac{\tilde{n}_{\nu_s}(t_0)}{H(z_0)}\, e^{-\Gamma_{\rm tot}\, t(z_0)}\,, \tag{27}$$

where $\tilde{n}_{\nu_s}(t_0)$ is the present number density of dark matter if it did not decay, $\Gamma_{\rm tot}$ is the total decay rate of the particle, z_0 is the redshift at which the photon was produced, and $t(z_0)$ is the age of the universe at z_0. A photon that has present energy E_γ was produced at redshift z_0 given by

$$1 + z_0 = \frac{m_s/2}{E_\gamma}\,. \tag{28}$$

Limits on the diffuse extragalactic background radiation (DEBRA; sometimes referred to as extragalactic background light [EBL]) can be used to constrain dark matter particles that produce a flux given by equation (27). Diffuse radiative decay constraints also were emphasized by Drees (2000) and Drees & Wright (2000) in papers that incorrectly estimate the relic density of singlet neutrinos (see Dodelson & Widrow 1994; Dolgov & Hansen 2000; AFP). A broadband limit was placed by Ressell & Turner (1989) on DEBRA. They found that the flux per unit solid angle must satisfy

$$d\mathscr{F}/d\Omega \lesssim (1\ {\rm MeV}/E_\gamma)\ {\rm cm}^{-2}\ {\rm sr}^{-1}\ {\rm s}^{-1}\,. \tag{29}$$

Shown in Figure 6 are these less constraining, yet broadband, bounds from Ressell & Turner (1989) for the $L_{\nu_\alpha} \approx 0$ case for singlet neutrino WDM.

Gruber (1992) found the form of the X-ray background to be

$$\frac{d\mathscr{F}}{d\Omega} \lesssim 7.9\ {\rm cm}^{-2}\ {\rm sr}^{-1}\ {\rm s}^{-1}\left(\frac{E_\gamma}{\rm keV}\right)^{-0.29} e^{-(E_\gamma/41\ {\rm keV})} \tag{30}$$

for energies of $\sim$3–60 keV and

$$\frac{d\mathscr{F}}{d\Omega} \lesssim 1650\ {\rm cm}^{-2}\ {\rm sr}^{-1}\ {\rm s}^{-1}\left(\frac{E_\gamma}{\rm keV}\right)^{-2.0} + 1750\ {\rm cm}^{-2}\ {\rm sr}^{-1}\ {\rm s}^{-1}\left(\frac{E_\gamma}{\rm keV}\right)^{-0.7} \tag{31}$$

from 60 keV to $\sim$6 MeV. These constraints are also shown in Figure 6 for the $L_{\nu_\alpha} \approx 0$ singlet WDM case.

Recently, the *Chandra X-Ray Observatory* (Hornschmeier et al. 2001; Tozzi et al. 2001) has resolved several structures that contributed to the unresolved X-ray background. They find that the resolved sources contributed from 60% to 90% of the previously unresolved background. We make a rough approximation from these considerations that at most $\sim$20% of the X-ray background described by Gruber (1992) may be due to a diffuse particle decay. The limits from this consideration are depicted in Figure 6 for the $L_{\nu_\alpha} \approx 0$ case.

However, these diffuse limits entail the implicit assumption that dark matter particles are not concentrated in objects but rather are *uniformly* distributed through space. This is certainly not the case, since structure has been at least somewhat clumped and nonisotropic in the sky since an epoch corresponding to a redshift of $z \gtrsim 10$. The limits on the singlet neutrino mass in the $L_{\nu_\alpha} \approx 0$ case obtained by

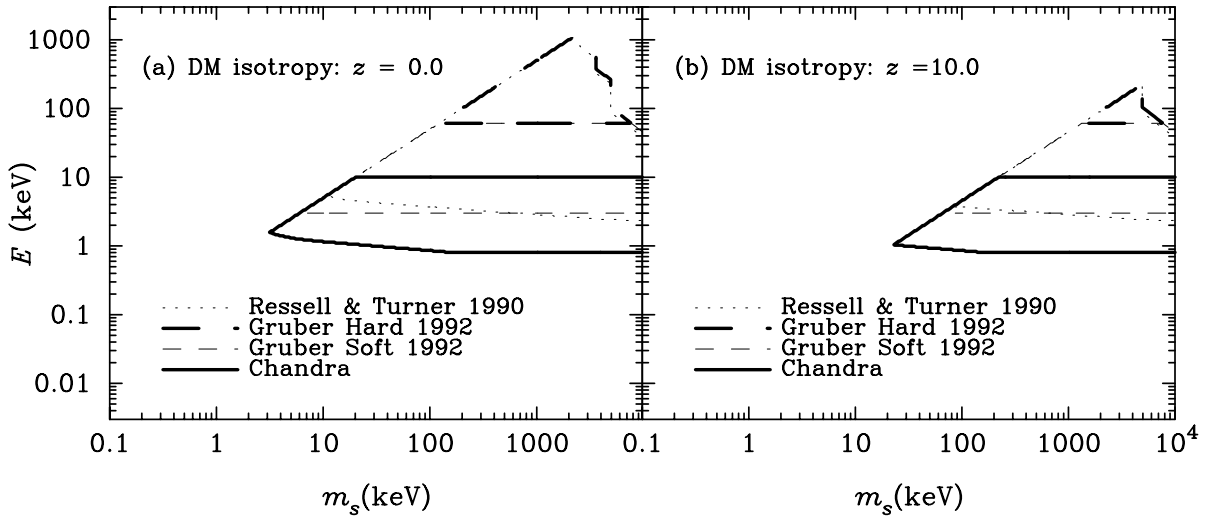

FIG. 6.—Limits on the diffuse flux from singlet neutrino decay in the $L_{\nu_\alpha} \approx 0$ case from photons produced at (*a*) $z \geq 0$ and (*b*) $z \geq 10$, assuming isotropy of the dark matter at that redshift.

an assumption of no clumping right up to the present ($z = 0$) epoch are shown in Figure 6*a*. This limit is roughly $m_s \lesssim 2$ keV. The limits for singlet dark matter in the $L_{\nu_\alpha} \approx 0$ case decaying at $z \gtrsim 10$, shown in Figure 6*b*, is approximately $m_s \lesssim 20$ keV. In this case the diffuse limit is greatly eased for the obvious reason that there is little diffuse dark matter at recent epochs. The true limit from a diffuse component should lie between these extreme cases. The actual limit depends on the epoch of significant structure formation and therefore on particular structure formation models.

6. CONCLUSIONS

We have argued that the serendipitous coincidence between the "sweet spot" for X-ray photon detection technology (photon energies between 0.5 and 10 keV on modern observatories like *Chandra* and *XMM-Newton*) and the structure consideration–preferred WDM particle rest mass range may afford an opportunity to detect or exclude a number of WDM candidates. Present observations of X-ray emission from clusters of galaxies (e.g., Virgo) may already nearly eliminate all but a small parameter region for the zero lepton number, nonresonant scattering production mode for singlet "sterile" neutrino WDM. We find that the nonobservance of a significant feature in deep observations of the central region of the Virgo Cluster excludes singlet neutrino WDM candidates with masses $m_s \gtrsim 5$ keV in the $L_{\nu_\alpha} \approx 0$ production mode.

However, exposures of large dark matter halos by current X-ray observatories could yield a spectral line for 2.5 keV $\lesssim m_s \lesssim 5$ keV (1.25 keV $\lesssim E_\gamma \lesssim 2.5$ keV) in the $L_{\nu_\alpha} \approx 0$ case unassociated with any atomic line. As detailed observations of the spatially resolved gas temperature profiles of rich clusters continue, accurate determinations of the dark matter profile in these clusters can be made, and existing limits and their uncertainties can be improved. Combined with lower mass bounds, upper limits from observation may exclude certain dark matter particle candidates.

The best strategy would be to target hot clusters or halos of spiral galaxies, which should have few emission lines in the energy range 1.25 keV $\lesssim E_\gamma \lesssim 2.5$ keV. In addition, the inferred existence of weakly lensing dark massive "blobs" (Clowe et al. 2001) provides a candidate for dark matter decay photon detection with relatively no background; however, the distance to such dark lenses is not well known, and therefore constraints on dark matter particle decay cannot be established from these objects.

The remaining (undetectable with ACIS on *Chandra*) $L_{\nu_\alpha} \approx 0$ parameter region is centered on $m_s \sim 1$ keV, the most interesting rest mass from a structure formation standpoint. Though this parameter space is already challenged by potential supernova core cooling effects (see, e.g., AFP), it would still be useful to close this window with another constraint venue.

The nonzero lepton number ($L_{\nu_\alpha} \neq 0$) cases for singlet neutrino WDM, corresponding to resonant production in the early universe (Shi & Fuller 1999; AFP) are not as yet detectable or constrainable with *Chandra*/*XMM*. However, the higher sensitivities that are possible with the Constellation X observatory could cover much of the interesting parameter space for these singlet neutrino models.

This is an exciting possibility. A line feature not attributable to an atomic line could be produced by the radiative decay of either singlet neutrinos, heavy active neutrinos, or gravitinos.

In any case, it is remarkable and unexpected that the hard-won technology of X-ray astronomy can in some cases probe a new regime of particle physics, one where particle interaction strengths are some 10 orders of magnitude weaker than the weak interaction. Put another way, modern X-ray observatories could probe epochs of the early universe corresponding to redshifts $z \sim 10^{12}$.

We would like to thank A. B. Balantekin, J. Bookbinder, D. O. Caldwell, G. Fossati, W. Heindl, M. Patel, R. Rothschild, and J. Tomsick for useful discussions. We would like to thank N. Dalal for suggesting nonluminous massive gravitational lenses as dark matter sources. This work was supported in part by NSF grant PHY 98-00980 at UCSD. K. A. would like to acknowledge support from a NASA GSRP fellowship. W. T. was supported in part by NASA contract NAS8-39073.

REFERENCES

Abazajian, K., Fuller, G. M., & Patel, M. 2001, Phys. Rev. D, 64, 023501 (AFP)
Abel, T., Anninos, P., Norman, M. L., & Zhang, Y. 1998, ApJ, 508, 518
Arkani-Hamed, N., Dimopoulos, S., & Dvali, G. 1998, Phys. Lett. B, 429, 263
Barger, V., Phillips, R. J. N., & Sarkar, S. 1995, Phys. Lett. B, 352, 365
Barkana, R., Haiman, Z., & Ostriker, J. P. 2001, ApJ, 558, 482
Binney, J., Gerhard, O., & Silk, J. 2001, MNRAS, 321, 471
Bode, P., Ostriker, J. P., & Turok, N. 2001, ApJ, 556, 93
Boehm, F., & Vogel, P. 1987, Physics of Massive Neutrinos (Cambridge: Cambridge Univ. Press)
Böhringer, H., et al. 2001, A&A, 365, L181
Brandt, N., et al. 2001, AJ, 122, 1
Bullock, J. S., Kravtsov, A. V., & Weinberg, D. H. 2001, ApJ, 548, 33
Caldwell, D. O. 1998, Int. J. Mod. Phys. A, 13, 4409
Cavaliere, A., & Fusco-Femiano, R. 1978, A&A, 70, 677
Clowe, D., Luppino, G., Kaiser, N., & Gioia, I. 2001, ApJ, 539, 540
Colombi, S., Dodelson, S., & Widrow, L. M. 1996, ApJ, 458, 1
Cowsik, R., & McClelland, J. 1972, Phys. Rev. Lett., 29, 669
Dalcanton, J. J., & Hogan, C. J. 2001, ApJ, 561, 35
Dicus, D. A., Kolb, E. W., & Teplitz, V. L. 1978, ApJ, 221, 327
Dine, M., Nelson, A. E., Nir, Y., & Shirman, Y. 1996, Phys. Rev. D, 53, 2658
Dodelson, S., & Widrow, L. M. 1994, Phys. Rev. Lett., 72, 17
Dolgov, A. D., & Hansen, S. H. 2000, preprint (hep-ph/0009083)
Drees, M. 2000, preprint (hep-ph/0003127)
Drees, M., & Wright, D. 2000, preprint (hep-ph/0006274)
Einasto, J., Kaasik, A., & Saar, E. 1974, Nature, 250, 309
Federspiel, M., Tammann, G. A., & Sandage, A. 1998, ApJ, 495, 115
Gerstein, S. S., & Zeldovich, Ya. B. 1966, Zh. Eksp. Teor. Fiz., 4, 174
Ghigna, S., Moore, B., Governato, F., Lake, G., Quinn, T., & Stadel, J. 2000, ApJ, 544, 616
Giudice, G. F., Kolb, E. W., & Riotto, A. 2001a, Phys. Rev. D, 64, 023508
Giudice, G. F., Kolb, E. W., Riotto, A., Semikoz, D. V., & Tkachev, I. I. 2001b, Phys. Rev. D, 64, 043512
Groom, D. E., et al. 2000, European Phys. J. C, 15, 1
Gruber, D. E. 1992, in The X-Ray Background, ed. X. Barcons & A. C. Fabian (Cambridge: Cambridge Univ. Press), 44
Hall, L. J., & Suzuki, M. 1984, Nucl. Phys. B, 231, 419
Horner, D. J., Mushotzky, R. F., & Scharf, C. A. 1999, ApJ, 520, 78
Hornschmeier, A. E., et al. 2001, ApJ, 554, 742
Kawasaki, M., Kohri, K., & Sugiyama, N. 2000, Phys. Rev. D, 62, 023506
Kawasaki, M., Sugiyama, N., & Yanagida, T. 1997, Mod. Phys. Lett. A, 12, 1275
Massó, E., & Toldrà, R. 1999, Phys. Rev. D, 60, 083503
Melott, A. L., Splinter, R. J., Persic, M., & Salucci, P. 1994, ApJ, 421, 16
Mikheyev, S. P., & Smirnov, A. Y. 1985, Soviet J. Nucl. Phys., 24, 913
Moore, B., Ghigna, S., Governato, F., Lake, G., Quinn, T., Stadel, J., & Tozzi, P. 1999, ApJ, 524, L19
Narayanan, V. K., Spergel, D. N., Davé, R., & Ma, C. 2000, ApJ, 543, L103
Navarro, J. F., Frenk, C. S., & White, S. D. M. 1995, MNRAS, 275, 720
———. 1996, ApJ, 462, 563
Nieves, J. F. 1983, Phys. Rev. D, 28, 1664
Ostriker, J. P., Peebles, P. J. E., & Yahil, A. 1974, ApJ, 193, L1
Pal, P. B., & Wolfenstein, L. 1982, Phys. Rev. D, 25, 766
Qian, Y., & Wasserburg, G. J. 2001, ApJ, 549, 337

Ressell, M. T., & Turner, M. S. 1989, Comments Astrophys., 14, 323
Sciama, D. W. 1990, ApJ, 364, 549
Sellwood, J. A. 2000, ApJ, 540, L1
Shi, X., & Fuller, G. M. 1999, Phys. Rev. Lett., 82, 2832
Shipman, H. L., & Cowsik, R. 1981, ApJ, 247, L111
Spergel, D. N., & Steinhardt, P. J. 2000, Phys. Rev. Lett., 84, 3760
Swaters, R. A., Madore, B. F., & Trewhella, M. 2000, ApJ, 531, L107
Takayama, F., & Yamaguchi, M. 2000, Phys. Lett. B, 485, 388
Tozzi, P., et al. 2001, ApJ, in press (astro-ph/0103014)
Valinia, A., et al. (The Constellation X Team). 1999, in AIP Conf. Proc. 470, After the Dark Ages: When Galaxies Were Young (the Universe at $2 < z < 5$): Ninth Astrophysics Conference, ed. S. S. Holt & E. P. Smith (Woodbury: AIP), 434
van Albada, T. S., Bahcall, J. N., Begeman, K., & Sancisi, R. 1985, ApJ, 295, 305
van den Bosch, F. C., Robertson, B. E., Dalcanton, J. J., & de Blok, W. J. G. 2000, AJ, 119, 1579
Weiner, B. J., Williams, T. B., van Gorkom, J. H., & Sellwood, J. A. 2001, ApJ, 546, 916
Willick, J. A., & Batra, P. 2001, ApJ, 548, 564
Wolfenstein, L. 1978, Phys. Rev. D, 17, 2369
Zwicky, F. 1933, Helvetica Phys. Acta, 6, 110

Note added in proof.—It should be noted that the three-neurtino decay processes of the singlet neutrino in Figure 1 (with the rate of eq. [7]) are possible only in the presence of a flavor-changing neutral current between neutrino flavors. We thank John Beacom for suggesting a clarification and emphasis of this point.